Report on Czech COSPAR-related activities in 2022-2023

This report summarizes selected results of Czech institutions represented in the Czech National Committee of COSPAR, namely the Institute of Atmospheric Physics (IAP) of the Czech Academy of Sciences (CAS), the Astronomical Institute (AI) of CAS, the Faculty of Mathematics and Physics of the Charles University (FMP CU), the Faculty of Electrical Engineering of the Czech Technical University, and the SME company Iguassu (space industry, representing the Czech Space Alliance). Both selected scientific results and Czech participation in space experiments are reported. There are also significant outreach/PR activities.

Participation in space experiments

Astronomical Institute of the Czech Academy of Sciences (AI CAS):

Solar Orbiter. AI CAS was involved in building three scientific instruments for the Solar Orbiter ESA mission: hard X-ray telescope STIX, coronagraph METIS and plasma wave detector RPW. For STIX, the flight power supply and on-board software was delivered. The main optics composed from two mirrors was designed and manufactured in collaboration with TOPTEC (part of the Institute of Plasma Physics of CAS) for the METIS telescope. Finally, a low-voltage power supply and corresponding power distribution unit was developed and manufactured at AI CAS for the RPW detector. Solar Orbiter was successfully launched on 10th of February 2020 and all the aforementioned instruments are working well.

ATHENA. In 2019, the Czech team became a member of the international instrumentation consortium of the X-ray Integral Field Unit (X-IFU), the main instrument planned for the ESA large X-ray mission ATHENA (Advanced Telescope for High Energy Astronomy). The X-IFU instrument will use a novel technique of X-ray calorimetry to precisely measure energies of X-ray photons. The international consortium is led by France and has 13 countries participating in the consortium. The Czech team is responsible for delivering a row-0 addressing module that will be part of warm electronics of the instrument. AI CAS is responsible for the project management and also for work in the X-IFU science advisory team. IAP CAS is responsible for the development of the electronics. In 2021, AI CAS got involved in development of the other detector onboard ATHENA mission, Wide Field Imager (WFI). The Czech team is responsible for the development of the Galvanic Isolation Modules.

LISA. The Czech Instrumental Group (CIG) joined the consortium of the large ESA gravitational-wave mission LISA (Laser Interferometer Space Antenna) in 2020. CIG is responsible for the development of the Fiber Switch Unit Actuators (FSUA). The FSUA uses piezo mechanisms to precisely rotate an optical element mounted in these mechanisms. By this rotation, the FSUA will be effectively able to switch between two sources of the laser beam, which guarantees the redundancy of the laser source. Since FSUA are critical elements for the LISA Optical Bench, CIG participates in the Interferometry Detection System of LISA mission. Apart from the mechanism itself, also the driving electronics and the box for the Mission Control Unit will be subject of the delivery. CIG involves four institutes of CAS: AI, Institute of Physics, IAP and Institute of Thermomechanics.

IXPE. The Czech scientific team is also involved in the exploratory NASA mission IXPE (Imaging X-ray Polarimetry Explorer) that was launched on 9th of December 2021. The Czech team is participating in the data analysis.

Juice. On JUICE mission the Czech team is a member of the international consortium for the Radio and Plasma Waves Instrument (RPWI). The responsibility of the ASU team was to perform the full development of a custom made low voltage power supply under very strict EMC requirements in order to provide reliable and unperturbed scientific measurements. The mission was successfully launched in 2023. We continue our activities in in-flight calibration, software development, and mission planning.

Swarm: Mission consisting of the satellite triplet launched in LEO orbit by ESA in 2013 with the main goal being the observation of Earth magnetic field. Given the excellent hardware health, currently the plans of the mission team is to cover by observations the current full solar cycle until 2031. Besides the magnetometers, the Swarm satellites also collect GPS data with sufficient precision to observe the variations in the gravity field at a spatial resolution of approximately 1500 km. These monthly gravity models, available from 2014 to the present, are independent of other gravimetric data sources, and although at a lower spatial resolution, this gravity time series is able to effectively bridge the 11-month gap between the Gravity Recovery and Climate Experiment (GRACE) and its Follow-On (GRACE-FO) missions and further short breaks in their data records. Given the good condition of the Swarm satellites, it is possible that they will continue to provide gravimetric information during potential gaps in GRACE-FO data, as well as for future dedicated gravimetric satellite missions. The Planetary Systems group of AI CAS is part of a consortium of five research institutions engaged in computing the Swarm gravity fields as an official mission product. The models are published every 3 months at ESA's Swarm Data Access server (https://swarm-diss.eo.esa.int/) as well at the International Centre for Global Earth Models (http://icgem.gfz-potsdam.de/series/02_COST-G/Swarm).

Institute of Atmospheric Physics of the Czech Academy of Sciences (IAP CAS):

We have continued our involvement in the development of new scientific spacecraft instrumentation. We have also worked on calibration and operations of spacecraft instruments and subsystems built by our team in the past.

In February 2020, the European Space Agency (ESA) launched a Solar Orbiter mission to the inner heliosphere. The spacecraft carries a Radio and Plasma Waves instrument (RPW) which includes a Time Domain Sampler (TDS) subsystem developed at the Institute of Atmospheric Physics in Prague. The instrument, including the TDS module, has been operating successfully since the beginning of the mission. We continued to run operations of the RPW instrument on Solar Orbiter.

The scientific and engineering team at IAP continued preparing an important hardware contribution to the future Comet Interceptor mission of ESA, which aims to investigate a dynamically new comet during its first approach to the Sun. IAP is developing a Dust and Data Processing Unit.

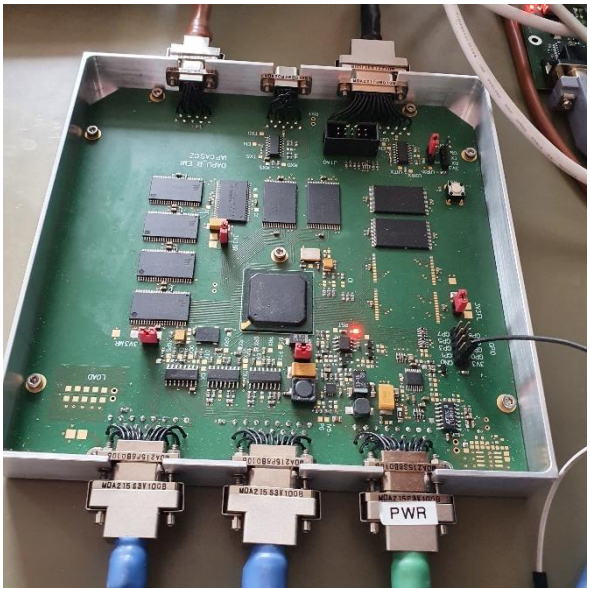

Fig. 2. A prototype of the DAPU data processing unit for the Dust, Field and Plasma instrument for the Comet Interceptor spacecraft.

IAP is Co-PI team in the RPWI (Radio and Plasma Waves Investigation) instrument of JUICE mission. The mission was launched in 2023, aiming at investigation of the Jovian system and its three Galilean icy moons (Europa, Ganymed and Callisto). We continue our activities in in-flight calibration, software development, and mission planning for the RPWI instrument on the spacecraft.

IAP is also involved in development of space electronics also for the large astrophysics missions of ESA, Athena and LISA, in collaboration with other institutes of the Czech Academy of Sciences.

Reception of the telemetry data of the WBD instrument onboard four ESA Cluster spacecraft continues in the Panska Ves station of the IAP. The data were processed at IAP CAS and submitted to international scientific community.

Faculty of Mathematics and Physics of the Charles University (FMP CU)

FMP CU participates in operation, health monitoring, data processing, and scientific interpretation of the SWA/PAS proton and alpha particle sensor data from the Solar Wind Analyzer suite onboard the ESA mission Solar Orbiter. After its launch the PAS sensors provided unique 3D ion velocity spectra with 4 s time resolution, that recently, after a SWA DPU software update has been improved to 1 or 2 s resolution depending on the PAS setup, allowing study plasma processes in the solar wind with unprecedented details.

Since 2019 FMP CU has been involved in the ESA Fast mission Comet Interceptor aiming to flyby near a dynamically new object (a comet or an extra-solar origin body). The mission has passed several review milestones being currently in the C/D implementation phase. In this mission we will provide part of the electronics of the electron spectrometer LEES (the 3D low-energy electron spectrometer led by IRAP Toulouse). The launch is currently planned in 2029.

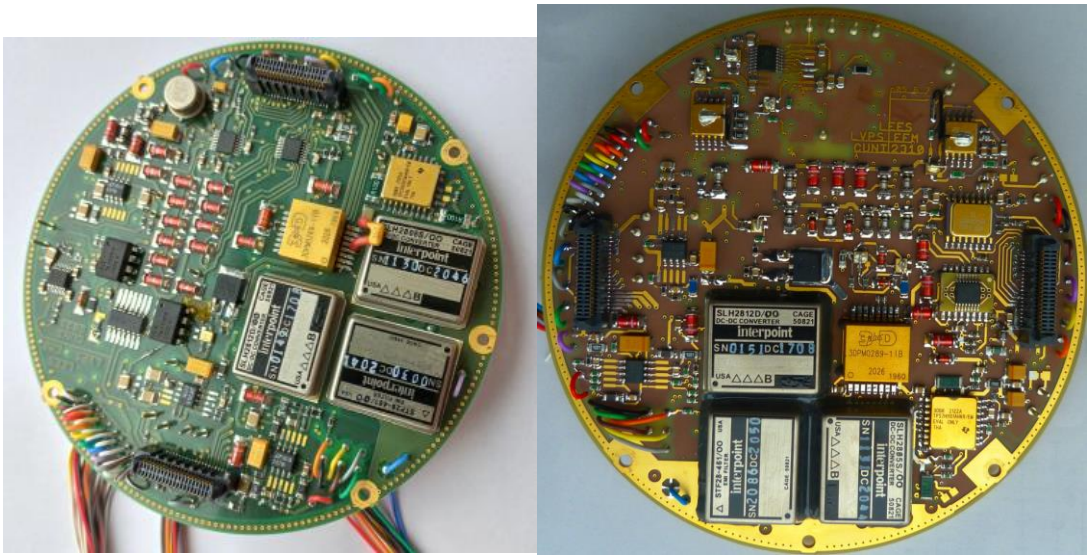

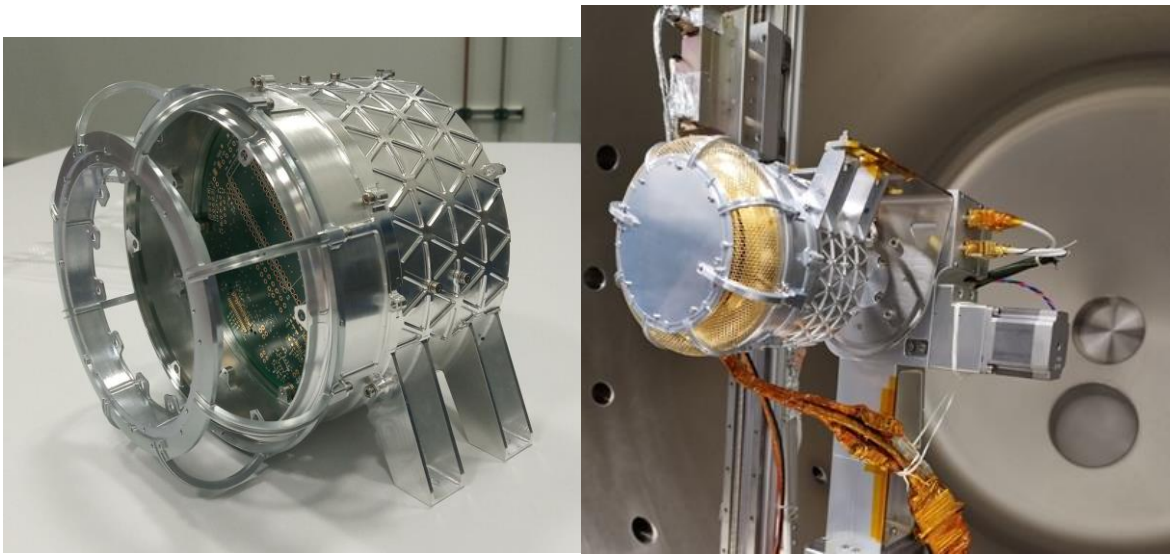

Fig. 3. The LEES low-voltage power supply EFM board developed at FMP CU and the LEES EM1 model during vacuum calibration in IRAP Toulouse.

During 2022-2023 FMP CU also worked on development of several Faraday-cup based solar wind monitor instruments (BMSW-LG for the Russian Luna-Resurs-1 OA) and a smaller version (FCA) for the Italian HENON cubesat mission (now in Phase C, expected launch 2027-2029).

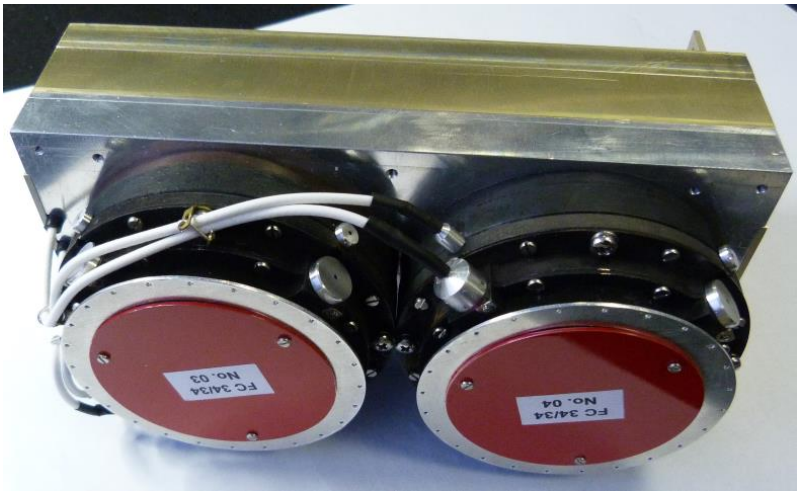

Fig. 4. Electronic module with a pair of Faraday cup detectors developed by Charles University for the modular BMSW-LG and FCA instruments.

Iguassu Software Systems, a.s.

We celebrated 15th anniversary of our accession to the ESA Convention (full ESA membership), attended by three Ministers, ESA Director General and other personalities. This event was followed by the annual Czech Space Week (CSW) in Brno. Apart from most of the Czech space industry and academia, we had a number of foreign visitors, principally from the neighbouring countries, but also as far as Japan.

After ongoing promotion of our space community in Japan by the Czech Space Alliance (CSA), Japanese space community is taking more interest in the Czech Republic. We had a visit of three representatives of JAXA, for whom we organised a seminar at the Ministry of

Transport, followed by presentations at the premises of our Japanese owned member, Rigaku, which showcased a number of joint projects with Japan by our academic and industrial entities. We also had a visit of a member of the board of IHI Aerospace and his colleague, with a similar programme. Another IHI representative followed up by attending the CSW in Brno. Further visits are planned for 2024. Recently, the honorary president of CSA returned to Tokyo to meet the Society of Japanese Aerospace Companies, to discuss conditions of attendance at the Japan Aerospace Exhibition 2024. Another objective was to secure support of our Embassy, the EU Japan Centre for Industrial Cooperation (EUJCIC) and a JAXA astronaut, to prepare a Czech space seminar in Tokyo in Oct. 2024.

We continue to participate in the EU Japan Business Round Table, to which CSA was nominated by EUJCIC.

The "Ambitious space projects" tender, issued by the Ministry of Transport, led to the selection of two national end-to-end satellite projects - one technological, the other scientific

Czech Republic presented itself at a national stand in Space-Tech Expo in Bremen.
As member of the Multi-GNSS Asia (MGA) we attended MGA conference in Thailand. We also attended the inauguration of the Thai Space Programme in Bangkok, the Space comm event in UK and EU Space week in Spain.

Thanks to the ongoing support of EUJCIC, we could present ourselves at their stand at International Space Industry Exhibition (ISIEX) Tokyo and we are invited to come back in 2024

In cooperation with the Ministry of Transport and the Czech Embassy, we continue talking to the Brazilian Space Agency, with which we have a LOI in space cooperation.

Selected scientific results

Institute of Atmospheric Physics of the Czech Academy of Sciences (IAP CAS):

Lightning at Jupiter pulsates with a similar rhythm as in-cloud lightning at Earth

Our knowledge about the fine structure of lightning processes at Jupiter was substantially limited by the time resolution of previous measurements. Recent observations of the Juno mission revealed electromagnetic signals of Jovian rapid whistlers at a cadence of a few lightning discharges per second, comparable to observations of return strokes at Earth. The duration of these discharges
was below a few milliseconds and below one millisecond in the case of Jovian dispersed pulses, which were also discovered by Juno. However, it was still uncertain if Jovian lightning processes have the fine structure of steps corresponding to phenomena known from thunderstorms at Earth. We therefore analyzed results collected by the Juno Waves instrument during 5 years of measurements at 125-microsecond resolution. We identified radio pulses with typical time separations of one millisecond, which suggested step-like extensions of lightning channels and indicated that Jovian lightning initiation processes were similar to the initiation of intracloud lightning at Earth.

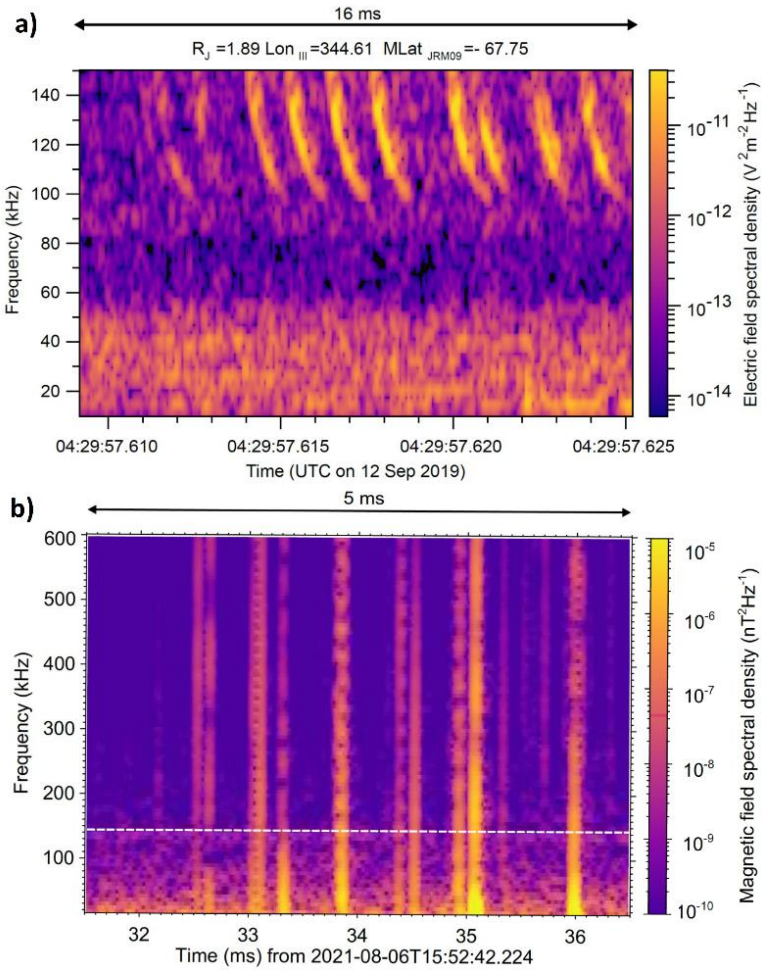

Fig. 5. a) Frequency-time spectrogram of power spectral density of electric field fluctuations of a group of dispersed pulses recorded by the Juno satellite on 12 September 2017 after 04:29:57 UTC at a radial distance of 1.89 RJ (Jovian radii). b) Frequency-time spectrogram of power spectral density of magnetic field fluctuations showing the 5 ms long detail of the initiation of an intracloud flash that occurred on 6 August 2021 at 15:52:42 UTC. The measurement was conducted by a broadband magnetic field antenna (5 kHz to 90 MHz) installed at the Dlouhá Louka observatory in Czechia. For comparison with the dispersed pulses from panel a), the white dashed line indicates the upper frequency limit of the Juno measurements.

Reference:

I. Kolmašová, O. Santolík, M. Imai, W. S. Kurth, G. B. Hospodarsky, J. E. P. Connerney, S. J. Bolton, **R. Lán** (2023). Lightning at Jupiter pulsates with a similar rhythm as in-cloud lightning at Earth. *Nature communications 14, 207*. Doi:10.1038/s41467-023-38351-6.

Related references:

Nature Research Highlights: Jupiter's lightning has rhythm — just like Earth's, 23 May 2023. Doi: 10.1038/d41586-023-01698-3.

Kurth, W. S., Wilkinson, D. R., Hospodarsky, G. B., **Santolík, O**., Averkamp, T. F., Sulaiman, A. H., et al.(2023). Juno plasma wave observations at Europa. *Geophysical Research Letters*, 50, e2023GL105775. Doi:10.1029/2023GL105775.

Theories of growth and propagation of parallel whistler-mode chorus emissions: A review

The significant role of nonlinear wave–particle interactions in the macrodynamics and microdynamics of the Earth's outer radiation belt has long been recognized. Electron dropouts during magnetic storms, microbursts in atmospheric electron precipitation, and pulsating auroras are all associated with the rapid scattering of energetic electrons by the whistler-mode chorus, a structured electromagnetic emission known to reach amplitudes of about 1% of the ambient magnetic field. Despite the decades of experimental and theoretical investigations of chorus and the recent progress achieved through numerical simulations, there is no definitive theory of the chorus formation mechanism, not even in the simple case of parallel (one-dimensional) propagation. We followed the evolution of these theories from their beginnings in the 1960s to the current state, including newly emerging self-consistent excitation models. A critical review of the unique features of each approach was provided, taking into account the most recent spacecraft observations of the fine structure of chorus. Conflicting interpretations of the role of resonant electron current and magnetic field inhomogeneity are discussed. We also discussed the interplay between nonlinear growth and microscale propagation effects and identify future theoretical and observational challenges stemming from the two-dimensional aspects of chorus propagation.

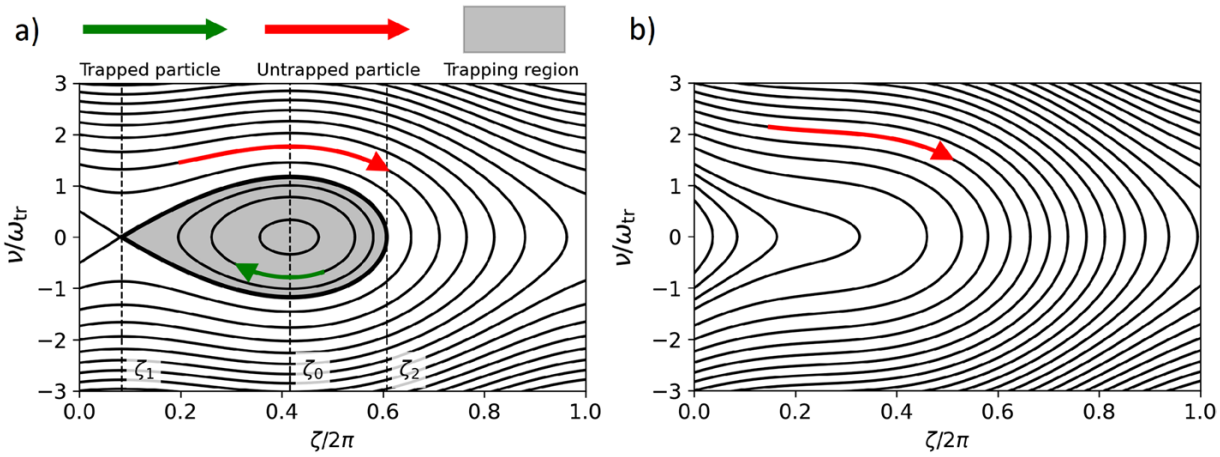

Fig. 6. Phase portrait showing the behaviour of electrons near cyclotron resonance with a constant inhomogeneity factor $S = -0.5$ (panel a) and $S = -1.2$ (panel b). Particles in the trapping region (green arrow) oscillate around a constant phase ζ_0 with respect to the circularly polarized electromagnetic field of chorus waves. Untrapped particles (red arrow) are not phase-locked.

Hanzelka, M. and **Santolík, O.** (2023). Theories of Growth and Propagation of Parallel Whistler-Mode Chorus Emissions: A Review, *Surveys in Geophysics*, Doi: 10.1007/s10712-023-09792-x.

Hartley, D. P., Christopher, I. W., Kletzing, C. A., Kurth, W. S., **Santolík, O., Kolmašová, I.**, et al. (2023). Chorus wave properties from Van Allen Probes: Quantifying the impact of the sheath corrected electric field. *Geophysical Research Letters, 50*. Doi:10.1029/2023GL102922.

Full-wave modeling of EMIC wave packets: ducted propagation and reflected waves

Electromagnetic ion cyclotron (EMIC) waves can scatter radiation belt electrons with energies of a few hundred keV and higher. To accurately predict this scattering and the resulting precipitation of these relativistic electrons on short time scales, we need detailed knowledge of the wave field's spatio-temporal evolution, which cannot be obtained from single spacecraft measurements.

Our study presented EMIC wave models obtained from two-dimensional (2D) finite-difference time-domain (FDTD) simulations in the Earth's dipole magnetic field. We studied cases of hydrogen band and helium band wave propagation, rising-tone emissions, packets with amplitude modulations, and ducted waves. We analyzed the wave propagation properties in the time domain, enabling comparison with in situ observations. We showed that cold plasma density gradients can keep the wave vector quasiparallel, guide the wave energy efficiently, and have a profound effect on mode conversion and reflections. The wave normal angle of unducted waves increases rapidly with latitude, resulting in reflection on the ion hybrid frequency, which prohibits propagation to low altitudes. The modeled wave fields can serve as an input for test-particle analysis of scattering and precipitation of relativistic electrons and energetic ions.

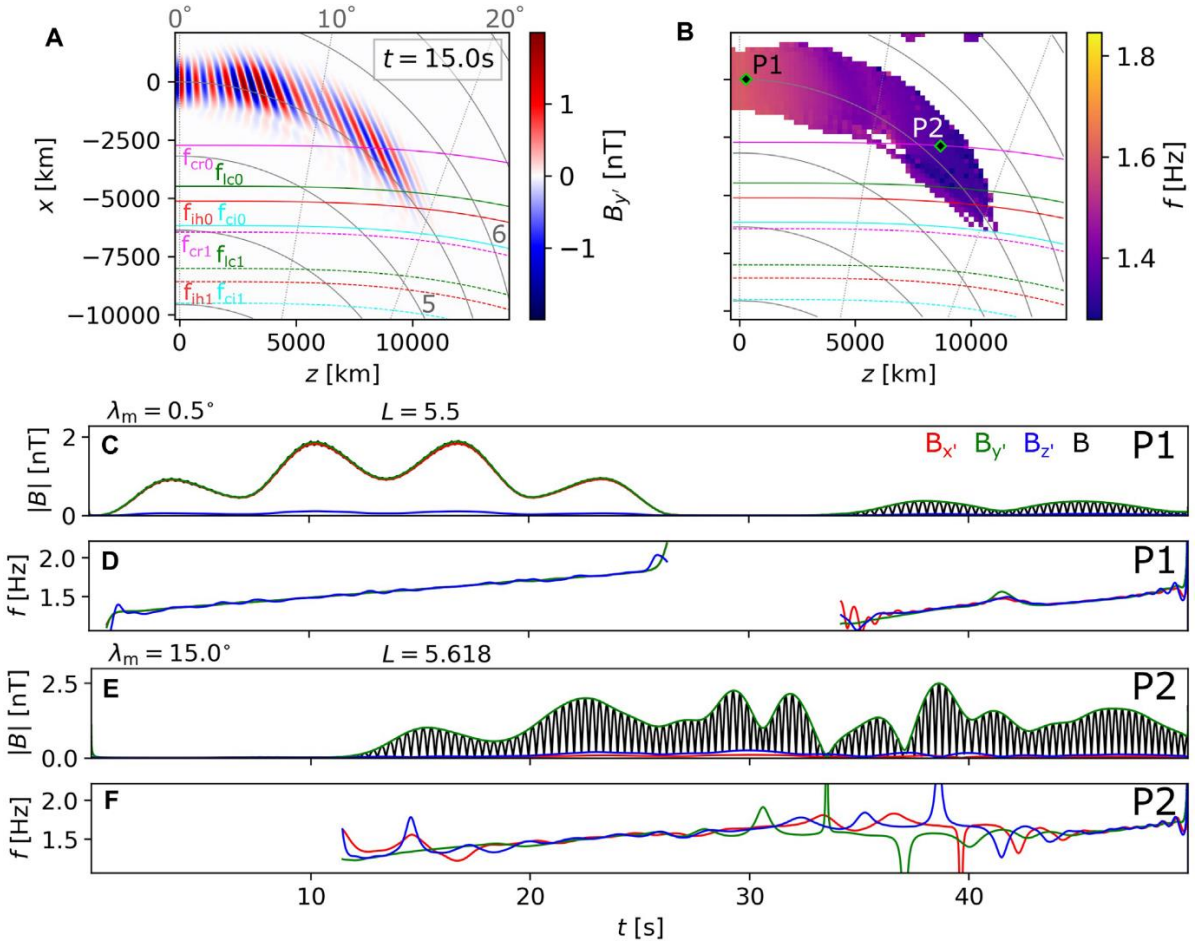

Fig. 7. Field components and propagation properties of waves from simulation run with input parameter Set 4 (rising-tone unducted hydrogen band wave packet with four subpackets). (A) Magnetic field component Bx' perpendicular to the local field line (perpendicular to the meridional plane). Snapshot taken at t = 15 s. Crossings of characteristic frequencies for wave at frequency ω_0 are represented by solid lines as before, and the crossing for the final

frequency ω_1 are plotted with dashed lines. (B) Instantaneous wave frequency snapshot, obtained as a power-weighted average of frequencies of the three magnetic components. Labels P1 and P2 show positions of probes that collected data analyzed in the following panels. (C) Probe P1 measured amplitude envelopes of the magnetic field components Bx', By', and Bz' plotted in red, green, and blue, respectively. The total magnetic field |B| is plotted with a black line. (D) Instantaneous frequencies from Probe P1, color coded as in the previous panel. (E, F) Same as panels (C, D), but with data from probe P2.

Hanzelka, M., Li, W., Ma, Q., Qin, M., Shen, X.-C., Capannolo, L., and Gan, L. (2023), Full-wave modeling of EMIC wave packets: ducted propagation and reflected waves. *Front. Astron. Space Sci.* 10:1251563. Doi: 10.3389/fspas.2023.1251563.

Parametric analysis of pitch angle scattering and losses of relativistic electrons by oblique EMIC waves

We analyzed the effects of electromagnetic ion cyclotron (EMIC) waves on relativistic electron scattering and losses in the Earth's outer radiation belt. EMIC emissions are commonly observed in the inner magnetosphere and are known to reach high amplitudes, causing significant pitch angle changes in primarily >1 MeV electrons via cyclotron resonance interactions. We run test-particle simulations of electrons streaming through helium band waves with different amplitudes and wave normal angles and assessed the sensitivity of advective and diffusive scattering behaviors to these two parameters, including the possibility of very oblique propagation. The numerical analysis confirmed the importance of harmonic resonances for oblique waves, and the very oblique waves are observed to efficiently scatter both co-streaming and counter-streaming electrons. However, strong finite Larmor radius effects limit the scattering efficiency at high pitch angles. Recently discussed force-bunching effects and associated strong positive advection at low pitch angles are, surprisingly, shown to cause no decrease in the phase space density of precipitating electrons, and we demonstrated that the transport of electrons into the loss cone balances out the scattering out of the loss cone. In the case of high-amplitude obliquely propagating waves, weak but non-negligible losses were detected well below the minimum resonance energy, and we identified them as the result of non-linear fractional resonances. Simulations and theoretical analysis suggested that these resonances might contribute to subrelativistic electron precipitation but are likely to be overshadowed by non-resonant effects.

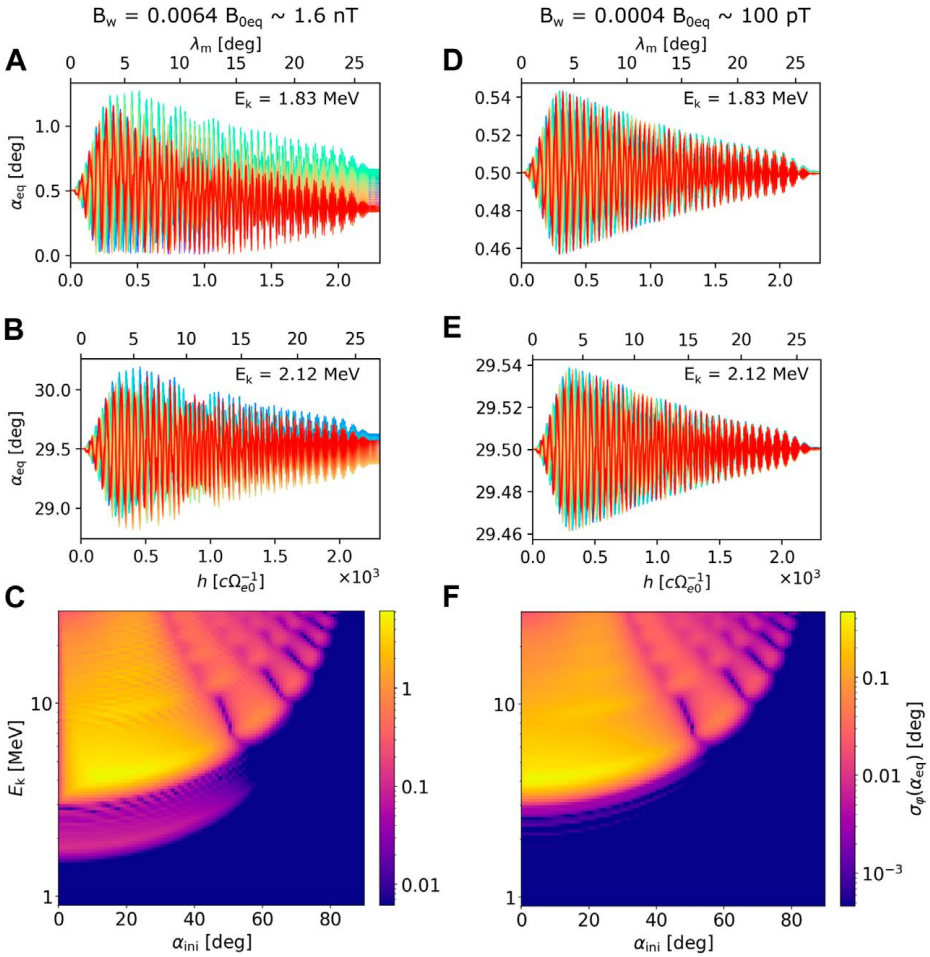

Fig. 8. Behavior of fractional resonances explained by particle trajectories and standard deviations in equatorial pitch angle for an EMIC wave with wave normal angle θ_k = 70° with respect to the background magnetic field (A–B) Changes in pitch angle along the field line at energies well below the equatorial fundamental resonance energy $E_{Rmin} \approx 4$ MeV. The wave amplitude is B_{w0} = 1.6 nT. (C) Standard deviation in equatorial pitch angle plotted in logarithmic scale that spans three orders of magnitude. Weak resonant effects near 2 MeV become apparent. (D–F) Same as (A–C) but for a 16 times smaller wave amplitude. The resonant effects near $E_{Rmin}/2$ are now insubstantial compared to the fundamental resonance.

Hanzelka, M., Li, W. and Ma, Q. (2023), Parametric analysis of pitch angle scattering and losses of relativistic electrons by oblique EMIC waves. *Front. Astron. Space Sci*. 10:1163515. Doi: 10.3389/fspas.2023.1163515.

A Strong Pulsing Nature of Negative Intracloud Dart Leaders Accompanied by Regular Trains of Microsecond-Scale Pulses

We reported the first observations of negative intracloud (IC) dart-stepped leaders accompanied by regular trains of microsecond-scale pulses, simultaneously detected by our shielded broadband magnetic loop antennas and the radio telescope Low Frequency Array (LOFAR). Four investigated pulse trains occurred during complicated IC flashes on 18 June 2021, when heavy thunderstorms hit the Netherlands. The pulses within the trains were unipolar, a few microseconds wide, and with an average inter-pulse interval of 5–7 μs. The

broadband pulses perfectly matched energetic, regularly distributed, and relatively isolated bursts of very high frequency sources localized by LOFAR. All trains were generated by negative dart-stepped leaders propagating at a lower speed than usual dart leaders. They followed channels of previous leaders occurring within the same flash several tens of milliseconds before the reported observations. The physical mechanism remains unclear as to why we observed dart-stepped leaders, which showed mostly regular stepping, emitting energetic microsecond-scale pulses.

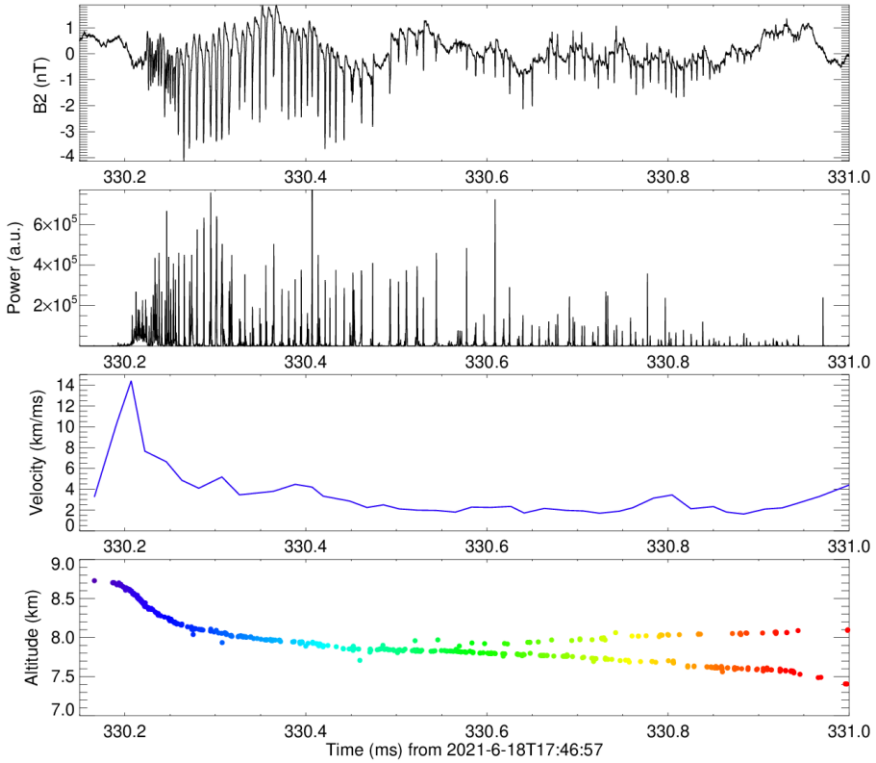

Fig. 9. Event C1: (a) Magnetic field pulse train measured by the Shielded Loop Antenna with a Versatile Integrated Amplifier (SLAVIA) antenna on 18 June 2021. (b) Very High Frequency (VHF) power detected at the same time by the Low Frequency Array (LOFAR) antenna CS002. (c) Average velocity of the leader movement. (d) Sources of VHF radiation located by the LOFAR impulsive imager.

Kolmašová, I., Scholten, O., **Santolík, O.**, Hare, B. M., Zacharov, P., **Lán, R.**, et al. (2023). A strong pulsing nature of negative intracloud dart leaders accompanied by regular trains of microsecond-scale pulses. *Geophysical Research Letters*, 50. Doi:10.1029/2023GL103864.

Quasiperiodic ELF/VLF emissions associated with corresponding pulsations of the geomagnetic field

We presented a comparison between properties of quasiperiodic (QP) extra low frequency/very low frequency emissions observed by the low-altitude DEMETER spacecraft and ultra-low frequency (ULF) geomagnetic field pulsations measured on the ground by the Canadian Array for Realtime Investigations of Magnetic Activity system of flux-gate magnetometers and by the Sodankylä Geophysical Observatory magnetometer. Altogether, we have analyzed 398 QP events observed at the times when DEMETER was close to the

ground-based magnetometers. The modulation periods of the analyzed QP events were larger than 10 s and their frequency bandwidths were larger than 200 Hz. For a part of QP emissions with modulation periods about 30 s, there was a good agreement between the modulation periods and peak frequencies of ULF magnetic field pulsations measured on the ground. These QP emissions appeared to be closely associated with coincident geomagnetic pulsations (QP1 type), and they represented ~18% of the total number of analyzed QP events. No corresponding geomagnetic pulsations were identified in the remaining 82% of QP events (QP2type). The intensity of QP1 events did not seem to correlate with the intensity of geomagnetic field pulsations, while the intensity of QP2 events increased with the integral intensity of geomagnetic field pulsations. Based on the observed association between QP emissions and geomagnetic field pulsations, we estimated the radial distance of the generation region of QP1 emissions to L ~ 7.

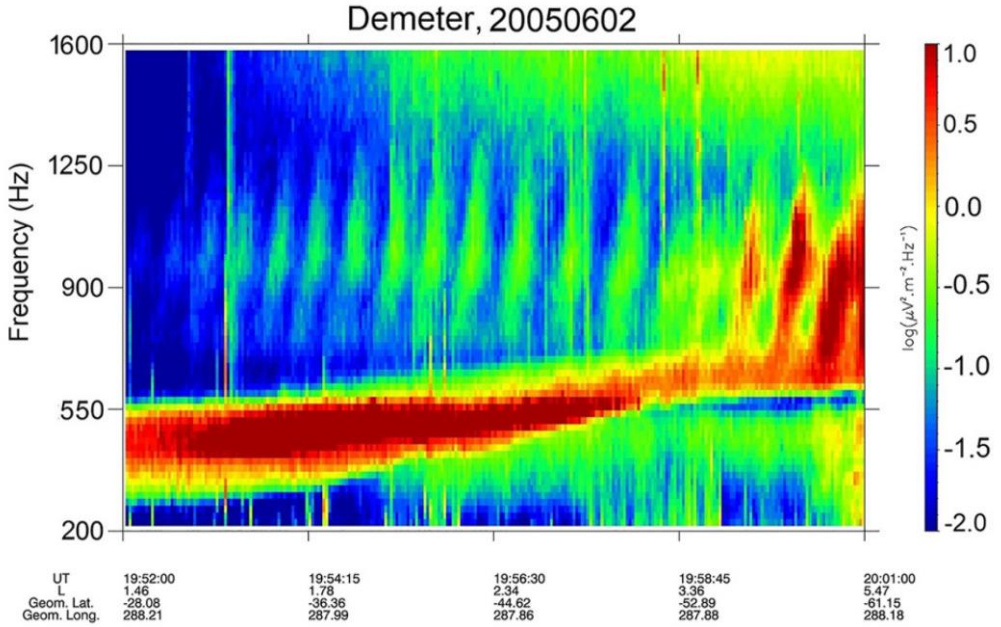

Fig. 10. Frequency-time spectrograms of power spectral density of electric field fluctuations corresponding to a quasiperiodic (QP) event measured on 2 June 2005 between 19.52 UT and 20:02 UT in the Southern hemisphere. A set of individual QP elements slowly fading out toward lower geomagnetic latitudes can be seen at frequencies between ~700 and ~1700 Hz.

Hajoš, M., Němec, F., Demekhov, A., **Santolík, O.,** Parrot, M., Raita, T., Bezděková, B. (2023), Quasiperiodic ELF/VLF emissions associated with corresponding pulsations of the geomagnetic field, *J. Geophys. Res. Space Phys.*, 128(4), e2022JA03110. Doi:10.1029/2022JA031103.

Classification of the spectral fine structure in auroral kilometric radiation

Auroral Kilometric Radiation (AKR) is generated by unstable energetic electron populations in the auroral region of Earth's magnetosphere. A mechanism known as the cyclotron maser instability amplifies weak background radiation at the expense of particle energy. However, this instability alone cannot explain frequent observations of AKR spectral fine structures when recorded with sufficiently high time and frequency resolution. We

analyzed observations of AKR from the Cluster Wideband Receiver and gave an overview of the different types of spectral fine structures found in this dataset in years 2002 and 2003. A classification scheme was introduced, and the occurrence rate for each class of fine structure was investigated in a statistical analysis. Possible generation mechanisms were discussed in relation to the observations.

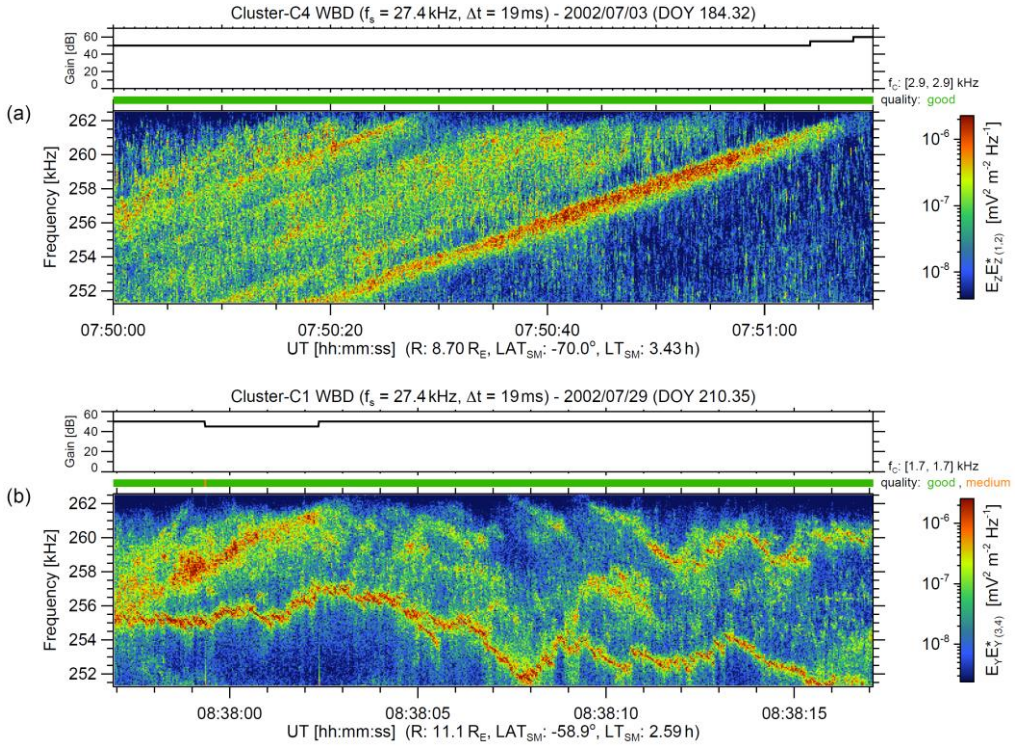

Fig. 11. (a) AKR Bands with a positive drift rate (∼0:22 kHz/s; ∼80 seconds displayed) and (b) irregularly drifting AKR Snakes (∼20 seconds displayed). The emission in (a) below the intensive bottom Band is AKR Rain (unresolved).

Taubenschuss, U., Fischer, G., **Píša, D., Santolík, O., Souček, J**. (2023). Classification of the spectral fine structure in auroral kilometric radiation, *C. K. Louis, C. M. Jackman, G. Fischer, A. H. Sulaiman, P. Zucca, Dublin Institute for Advanced Studies (Eds.), Planetary, Solar and Heliospheric Radio Emissions IX*. Doi:10.25546/103089.

Contribution to development of the International Reference Ionosphere – incorporation of the new global model of the ion temperature

Our newly developed global model of the ion temperature (Ti) (TBKST-2021) has been accepted as an "option" for the ion temperature in the International Reference Ionosphere (IRI) model (Bilitza et al., 2022). The model has been implemented in FORTRAN, the language in which the entire IRI model is written, and has been incorporated into the code of the latest version of IRI, IRI-2020. IRI-2020, including earlier versions, is available at irimodel.org. Bilitza et al. 2022 provide an overview and description of other submodels or options for the latest version of IRI, including our previously developed ones for ion composition (TBT15) and electron temperature (TBT-2012).

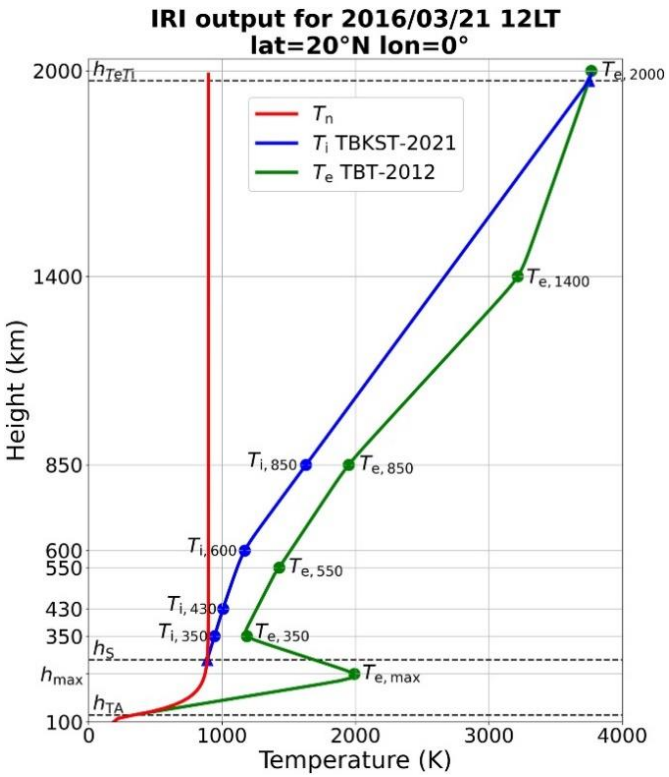

Fig. 12. An example of vertical profiles of the ion temperature (blue) in comparison with the temperature of neutral atmosphere (Tn) (red) and electron temperature (green) as follows from IRI-2020 and TBKST-2021, NRLMSISE-00 a TBT-2012 options for individual parameters in the altitude range of about 100 – 2000 km. Solid circles indicate altitudes (called anchor points) used in IRI-2020 to model gradient changes in temperature profiles. Dashed lines denote characteristic heights h_{TA}=120 km, h_s, and h_{TeTi} also used in the IRI-2020 model for construction of temperature vertical (height) profiles.

Bilitza, D., Pezzopane, M., **Truhlik, V**., Altadill, D., Reinisch, B. W., Pignalberi, A., 2022: The International Reference Ionosphere Model: A Review and Description of an Ionospheric Benchmark, Reviews of Geophysics, 60, 4, https://doi.org/10.1029/2022RG000792

Larger-scale gravity waves seen in mesospheric and ionospheric data can be generated by the movement of the tropospheric frontal system of the continental scale

Mesospheric and particularly ionospheric effects have been studied of two tropospheric mesoscale situations caused by exceptional synoptic-scale circulation conditions enhanced by the influence of the local convective environment. We found that spread-F echo occurs after frontal passage due to orographically enhanced jet stream, which also cases irregularities on ionograms. Distortion of diurnal foF2 and hmF2 distributions is observed during both events. Increase in the detected amplitude of horizontal plasma flow and changes in vertical plasma drifts are registered during event days. Wavelike oscillations in the gravity wave (GW) mode develop in ionospheric parameters. Increase in GW activity in the mesosphere is detected before and around the analyzed events. A majority of waves observed in the mesosphere occur during the night before the cold front reaches the observational point. Identified GW structures in the mesosphere propagate into a wide range of directions; no prevailing direction

can be identified. Large-scale and small-scale GW structures are observed in the mesosphere during cyclonic event. Only small-scale GW structures are registered in the mesosphere in relation to the polar front jet stream situation.

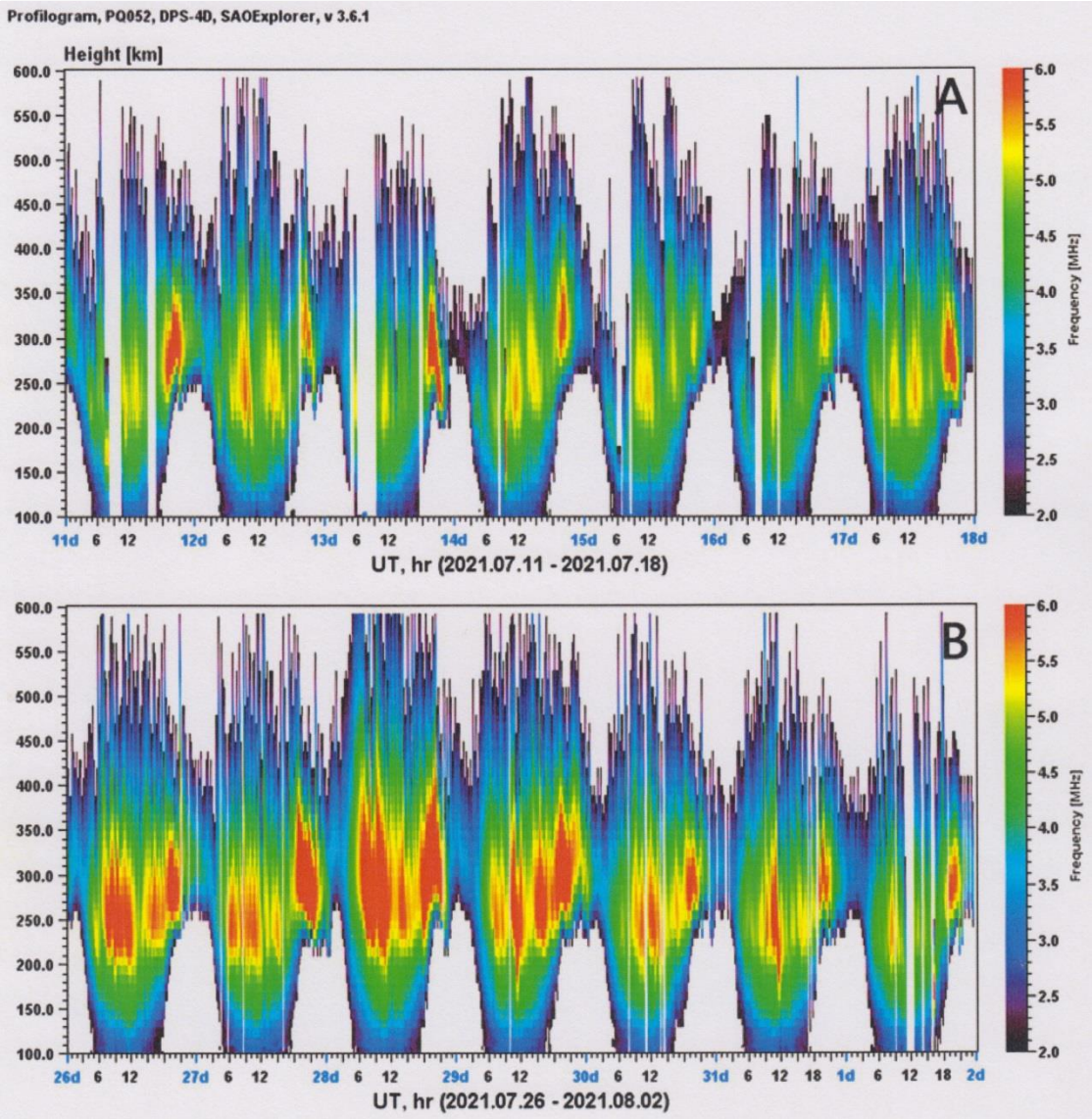

*Fig. 13. Profilograms obtained from full electron concentration profiles (manuaaly scaled ionograms) for a cyclonic event **(A)** and polar front jet stream **(B)**. Profilograms indicate that ionization within the whole F-layer ionosphere is higher during the jet stream event on 29 July 2021 **(B)** than ionization around mid-July 2021 **(A)**. In both cases, oscillations in the gravity wave domain are well observed during the entire studied time span.*

Koucka Knizova, P., Potuznikova, K., Podolska, K., Hannawald, P., **Mosna, Z., Kouba, D., Chum, J**., Wüst, S., Bittner, M., **Kerum, J.**, 2023: Multi-instrumental observation of mesoscale tropospheric systems in July 2021 with a potential impact on ionospheric variability in midlatitudes. Front. Astron. Space Sci., 10, https://doi.org/ 10.3389/fspas.2023.1197157 .

F30 is the best solar activity proxy for long-term ionospheric investigations.

To study ionospheric climate, to model the ionosphere and to investigate its long-term changes and trends, solar activity proxies/indices have been used, because long and homogeneous data series of solar ionizing flux are not available. To identify the optimum solar activity proxies, we use yearly average foF2 data of 6 representative ionospheric stations from middle latitudes of four continents over 1976-2014 and six solar activity proxies, F10.7, sunspot numbers, F30, Mg II, He II, and solar H Lyman-a flux. Four criteria were applied: (1) the largest percentage of foF2 variance described by solar proxy, (2) the smallest average absolute difference between observed and from solar proxy calculated foF2, (3) the highest temporal stability of dependence of foF2 on solar proxy, (4) the best stability of long-term of foF2 computed with the use of different solar proxies at different stations. F30 is found to be clearly the best solar proxies for variability of foF2 at middle latitudes according to the above criteria, not the usually used F10.7 or sunspot numbers, **which means change of paradigem**. Only F30 provides for all six stations and two sub-periods the same signs of trends; other solar activity proxies not. We recommend for investigating the midlatitude yearly values of foF2 the solar proxy F30, not the traditional F10.7 or sunspot numbers. F30 should be applied also in ionospheric modeling and climatological studies.

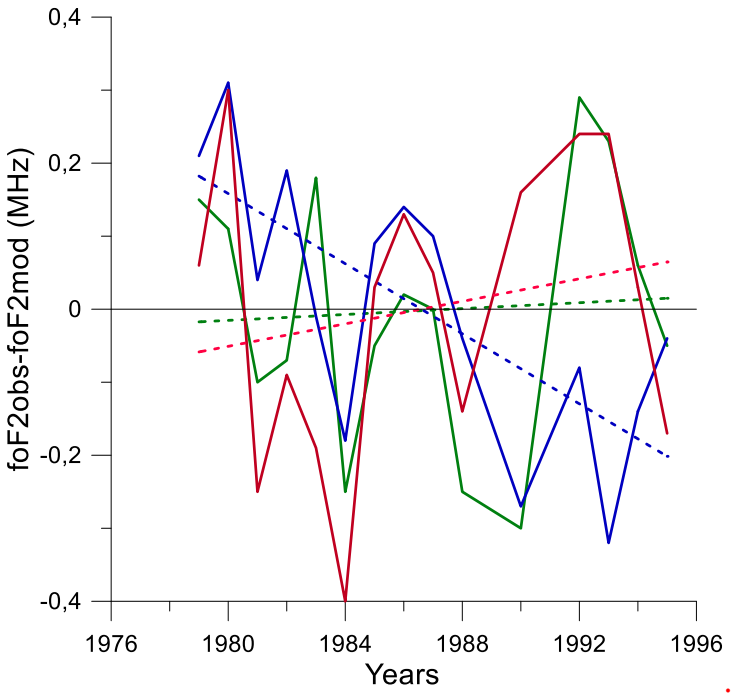

Fig. 14. Trends in foF2 in terms of foF2 residuals (differences between observed and from solar proxy calculated foF2) for Boulder, 1979–1995. Full lines – foF2 residuals; dashed lines – corresponding foF2 linear trends (fits). Green line with F10.7 applied to remove solar activity effect, red line with Mg II and blue line with F30. Long horizontal black thin line – zero level (no trend).

Lastovicka, J., Buresova, D., 2023: Relationships between foF2 and various solar activity proxies. Space Weather, 21 (4), e2022SW003359, doi: 10.1029/2022SW003359.

Lastovicka, J., 2024: Dependence of long-term trends in foF2 at middle latitudes on different solar activity proxies. Advances in Space Research, 73 (1), 685-689, https://doi.org/10.1016/j.asr.2023.09.047.

Atmospheric and ionospheric waves induced by Hunga Tonga eruption

The massive explosive eruption of the Hunga volcano on 15 January 2022 generated atmospheric waves that were recorded around the globe and which affected the ionosphere. This study builds on detection of ionospheric motions at specific altitudes using continuous Doppler sounding. Much attention is paid to long-period infrasound, which is in Europe observed simultaneously in the troposphere and ionosphere about an hour after the arrival of the first horizontally propagating pressure pulse (Lamb wave). It propagated approximately along the shorter great circle path over a distance ~16000 km. An unusually large traveling ionospheric disturbance (TID) was observed in Europe in association with the pressure pulse from the Hunga Tonga eruption. Doppler sounders in East Asia, South Africa and South America did not record such a significant TID. However, TIDs were observed in East Asia around times when Lamb waves passed the magnetically conjugate points. Figure XXX shows two infrasonic waves arriving along the shorter great circle pass and later in opposite direction along the longer great circle path.

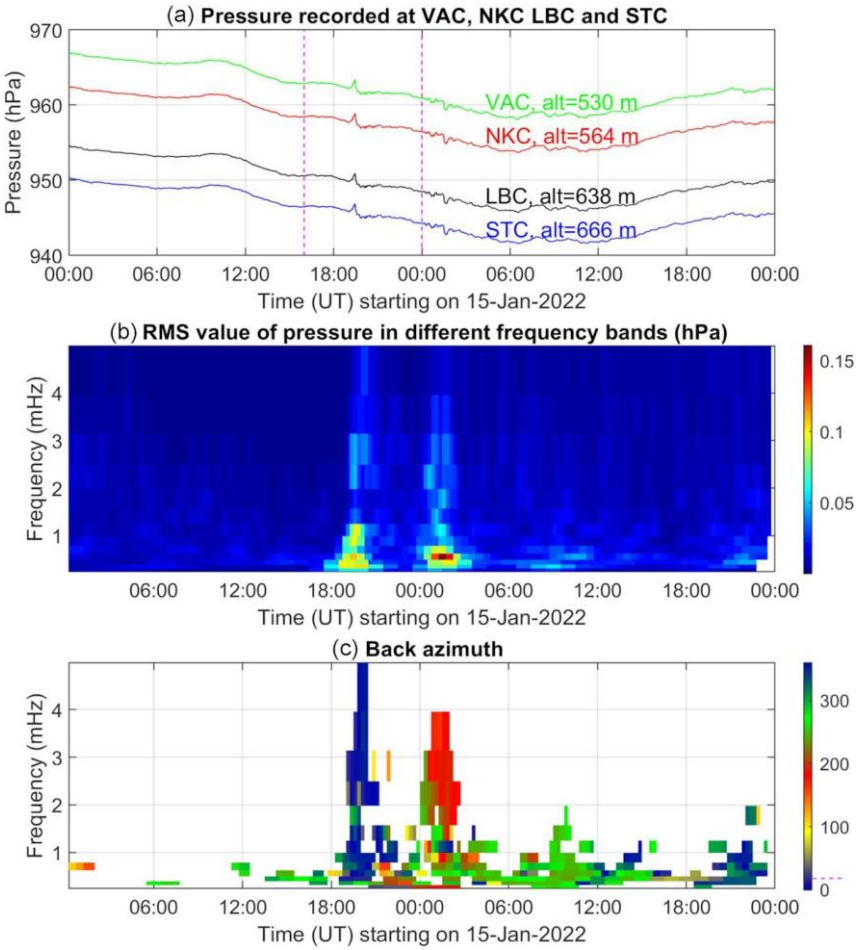

Fig. 15. (a) Pressure recorded by each site of the WBCI microbarometer array in western Czechia on 15 and 16 January 2022. (b) Dynamic spectrum of respective pressure fluctuations averaged over the WBCI sensors. (c) Back-azimuth of propagating waves displayed as a function of period and time.

Chum, J., Sindelarova, T., Koucka Knizova P. et al., 2023: Atmospheric and ionospheric waves induced by the Hunga eruption on 15 January 2022; Doppler sounding and infrasound. Geophys. J. Int., 233 (2), 1429–1443, https://doi-org /10.1093/gji/ggac517.

Astronomical Institute of the Czech Academy of Sciences (AI CAS):

Swarm internal geomagnetic field

Based on Swarm L2 data products the behaviour of the peculiar spectral area of the internal geomagnetic field was studied. Iteratively from the satellite altitude a given full geomagnetic spectrum of the internal field was split into the main/core and the lithospheric parts. This splitting does not use a traditional cut-off degree that would sharply distinguish the core and the lithospheric fields, but the two fields are obtained iteratively due to natural attenuation from a satellite altitude (see the figure, where the green and red lines continue in the trend given by the dashed line - the lithospheric field naturally arises from the total field as a residual with a smooth spectral transition).

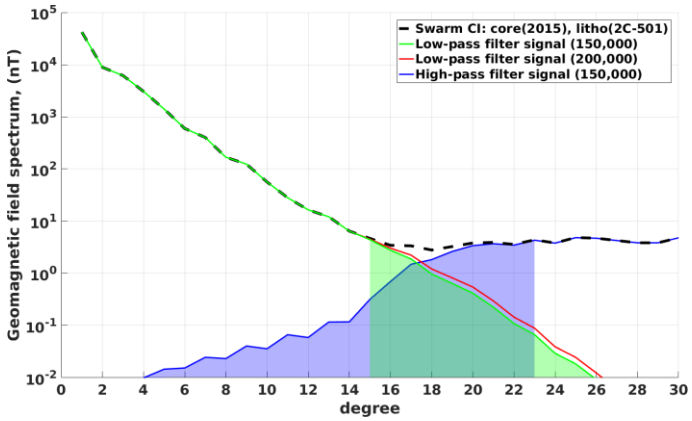

Fig. 16. Geomagnetic field spectra of the internal field from Swarm data (dashed line) and the output fields for two maximum numbers of iterations (green and red lines). The blue line represents the residual field (magnetic anomaly) obtained for 150,000 iterations. The shaded areas emphasize the power that cannot be reached by using cut-off degrees (from Sebera et al., 2022).

Sebera J, Bezděk A, Ebbing J, 2022. Satellite magnetic anomalies with a smooth spectral transition to long wavelengths. Physics of the Earth and Planetary Interiors 324, 106843. https://doi.org/10.1016/j.pepi.2022.106843

Faculty of Mathematics and Physics of the Charles University (FMP CU):

Magnetospheric Line Radiation Observed Close to the Source.

Magnetospheric Line Radiation (MLR) is a type of whistler mode electromagnetic wave phenomenon observed in the inner magnetosphere at frequencies of a few kilohertz that is characterized by a frequency modulation of the wave intensity. Although such events are

quite regularly observed by ground-based stations and low-altitude spacecraft, their observations in the equatorial region at larger radial distances (i.e., close to tentative source regions) are extremely limited, likely due to the generally low frequency resolution of available measurements. A systematic search for MLR in continuous intervals of high-resolution multicomponent wave data obtained by the Van Allen Probes spacecraft detects 15 events that occurred primarily on the dayside at frequencies between about 1 and 5 kHz, propagating with oblique wave normals away from the geomagnetic equator. For one event, simultaneous ground-based observations have been identified, providing limits on the spatial extent of the event – not beyond the high-density plasmasphere region. An electrostatic wave at a frequency corresponding to the modulation frequency of MLR was observed during some three events, likely linked to the event formation mechanism and not observed before.

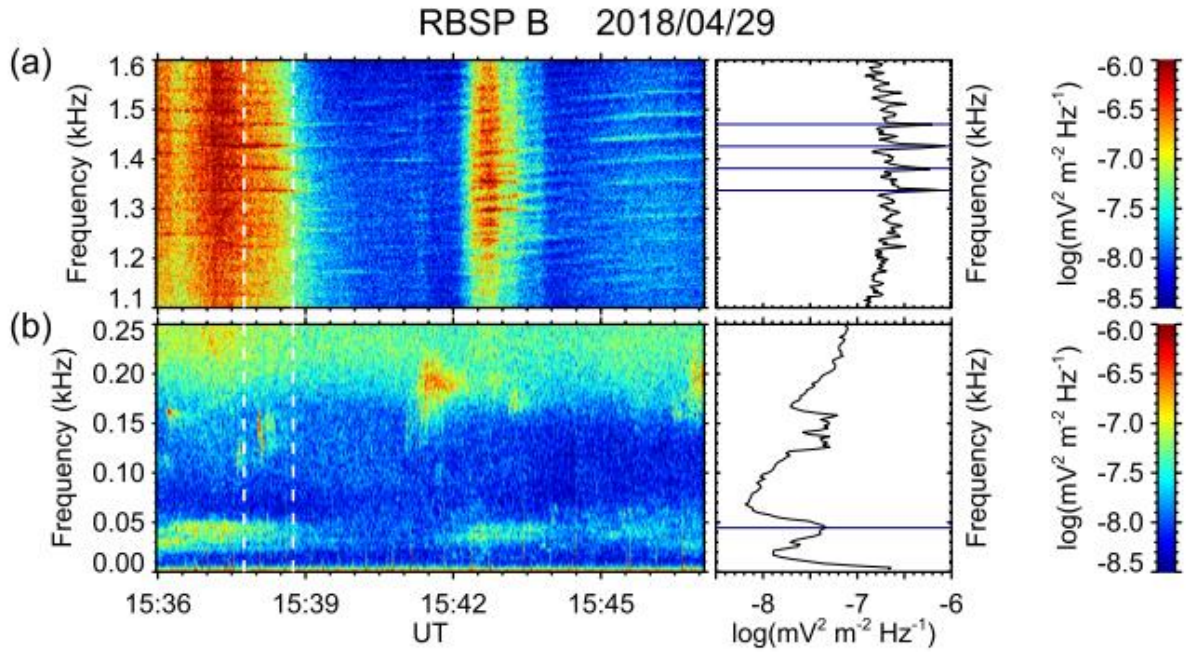

Fig. 17. Data obtained by Radiation Belt Storm Probes B on 29 April 2018. The left column shows frequency-time spectrograms of power spectral density of electric field fluctuations and the right column shows the corresponding frequency spectra. (a) Frequencies between 1,100 and 1,600 Hz, where the Magnetospheric Line Radiation (MLR) event is observed. (b) Frequencies between 0 and 250 Hz, revealing a wave at a frequency corresponding to the frequency spacing of the MLR event.

Němec, F., Manninen, J., **Santolík, O**., Hospodarsky, G. B., & Kurth, W. S. (2023). Magnetospheric line radiation observed close to the source: Properties and propagation. *Journal of Geophysical Research: Space Physics,* 128, e2023JA031454. https://doi.org/10.1029/2023JA031454.

Evolution of Magnetic Field Fluctuations and Their Spectral Properties within the Heliosphere: Statistical Approach

The authors present the first comprehensive statistical study of the evolution of compressive and non-compressive magnetic field fluctuations in the inner heliosphere. Based on Parker Solar Probe (PSP) and Solar Orbiter data at various distances from the Sun, the

general trend is shown and data compared with Wind observations near 1 au. The paper analyzes solar wind power spectra of magnetic field fluctuations in the inertial and kinetic ranges of frequencies. A systematic steepening of the spectrum in the inertial range with the spectral index of around −3/2 at closest approach to the Sun toward −5/3 at larger distances (above 0.4 au) has been found, the spectrum of the field component perpendicular to the background field being steeper at all distances. In the kinetic range, the spectral indices increase with distance from −4.8 at closest PSP approach to ≈−3 at 0.4 au and this value remains approximately constant toward 1 au. It is shown that the radial profiles of spectral slopes, fluctuation amplitudes, spectral breaks, and their mutual relations undergo rapid changes near 0.4 au.

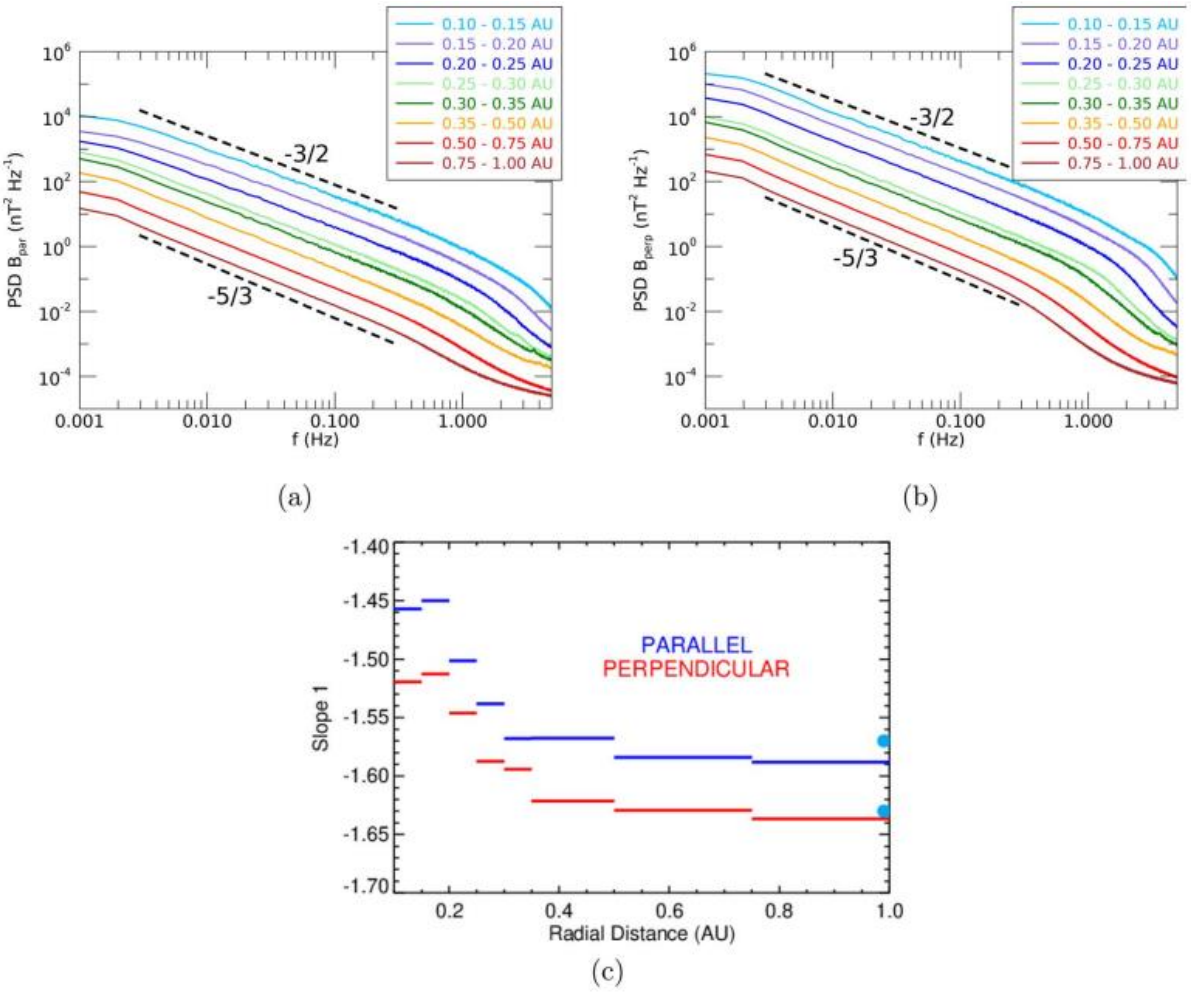

Fig. 18. Median PSD spectra of (a) compressive and (b) non-compressive magnetic field fluctuations in different distance bins from the Sun (in the spacecraft frame); (c) Variations of the magnetic field spectral index as a function of heliocentric distance in the inertial range (10^{-2} –10^{-1} Hz). The light blue points indicate the values of the slopes in the large statistics of Wind data (Šafránková, 2019).

Šafránková J., Němeček Z., Němec F., Verscharen D., Horbury T.S., Bale S.D., **Prech L**. (2023). Evolution of Magnetic Field Fluctuations and Their Spectral Properties within the Heliosphere: Statistical Approach. *The Astrophysical Journal Letters*, 946:L44. https://doi.org/10.3847/2041-8213/acc531.

Laboratory Simulation of the Positron–Dust Interaction and its Implication for Interstellar Dark Clouds

The authors report on the first laboratory experiment dealing with the interaction of a cosmic dust simulant with positrons emitted from a ^{22}Na radioisotope. Measurements of a charge of micrometer SiO^2 dust grains with an accuracy of one elementary charge *e* revealed +1 *e* steps due to positron annihilation inside the grain. The observed average rate of these charging events agrees well with prediction of a model based on the continuous slowing down approximation of energetic of positrons inside the grain. Less frequent charge steps larger than +1 *e* were attributed to emission of secondary electrons during positron slowing down.

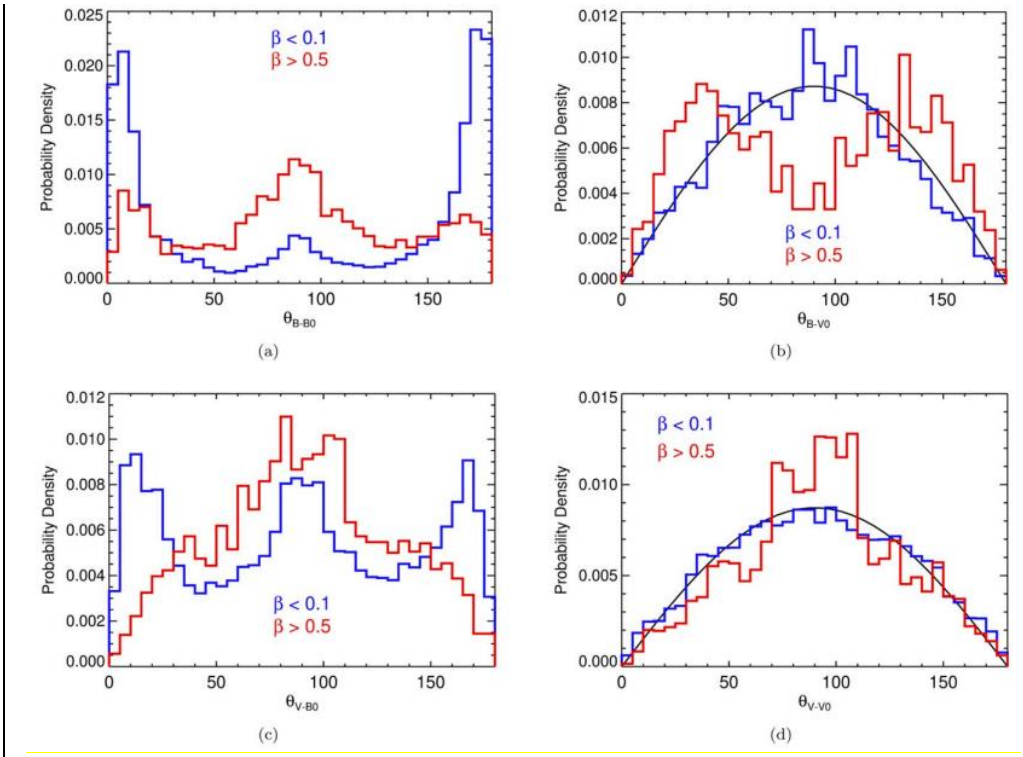

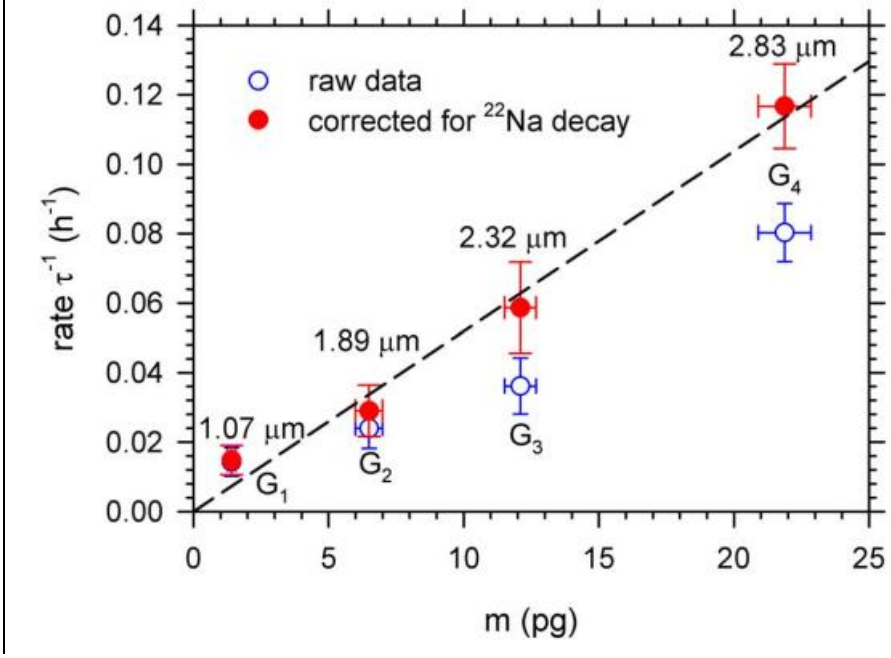

Fig. 19. The average rates between charging events, τ^{-1} , measured for grains G1–G4 plotted as a function of the grain mass, m. In order to compare results for the same activity of the positron source, the measured rates, τ^{-1} , plotted by open symbols, are corrected for the decay of the ^{22}Na source and corrected rates, $(\tau^*)^{-1}$, are plotted by red full symbols.

The determined coefficient of secondary electron emission is approximately inversely proportional to the grain radius. The experimental results led the authors to the formulation of a possible scenario of interstellar dark clouds charging.

Wild J., Čížek J., Nouzák L., Pavlů J., Šafránková J., Němeček Z., Vaverka J., Nosek D., Burian T., Wildová A., and Broulím J. (2023). Laboratory Simulation of the Positron–Dust Interaction and its Implication for Interstellar Dark Clouds. *The Astrophysical Journal*, 942:42. https://doi.org/10.3847/1538-4357/aca01c.